Journal of Applied Polymer Science

Preparation and Characterizations of Superparamagnetic Iron Oxide-Embedded Poly(2-hydroxyethyl methacrylate) Nanocarriers

Meher Kanta Gupta, Jaya Bajpai, Anil Kumar Bajpai
Department of Chemistry, Bose Memorial Research Laboratory, Government Autonomous Science College, Jabalpur, Madhya Pradesh 482002, India
Correspondence to: A. K. Bajpai (Email: akbmrl@yahoo.co.in or akbajpailab@yahoo.co.in)

ABSTRACT: The present study aims at formulating a novel multifunctional biocompatible superparamagnetic nanoparticles carrier system with homogeneously dispersed magnetic material in solid polymer matrix of poly(2-hydroxyethyl methacrylate) (PHEMA). The nanocomposites were designed by modified suspension polymerization of 2-hydroxyethyl methacrylate followed by *in situ* coprecipitation of iron oxide inside the nanoparticle matrix yielding magnetic PHEMA (mPHEMA) nanocomposites. The so prepared nanocomposites were characterized by Fourier transform Infrared spectroscopy, X-ray diffraction technique, Raman spectroscopy, electron diffraction, and energy-dispersive X-ray spectroscopy confirming the presence of Fe_3O_4 inside the PHEMA nanoparticles. The magnetization studies of nanocomposites conducted at room temperature using vibrating sample magnetometer suggested for their superparamagnetic nature having saturation magnetization (Ms) of 20 emu/g at applied magnetic field of 5 kOe. Transmission electron microscopy, field-emission scanning electron microscopy, and dynamic light scattering/zeta potential measurements were also performed which revealed that size of mPHEMA nanocomposites was lying in the range of 60–300 nm having zeta potential of −93 mV. The nanocomposites showed no toxicity as revealed by cytotoxicity test performed on L-929 fibroblast by extract method. The results indicated that the prepared superparamagnetic mPHEMA nanocomposites have enormous potential to provide a possible option for magnetically assisted targeted delivery of anticancer drugs. © 2014 Wiley Periodicals, Inc. J. Appl. Polym. Sci. **2014**, *131*, 40791.

KEYWORDS: biocompatibility; biomedical applications; composites; nanostructured polymers; radical polymerization

Received 25 December 2013; accepted 31 March 2014
DOI: 10.1002/app.40791

INTRODUCTION

Nanocomposites can be defined as multiphase solid materials in which at least one phase has one, two or three dimensions of nanosize range, or structures having nanoscale repeat distances between the different phases of the material.[1] The properties of nanocomposites depend not only on the individual parent components but also on their morphology and interfacial characteristics. The interactions between the filler components of nanocomposites at nanometer scale enable them to act as molecular bridges in the polymer matrix and create new properties for the composite material. Among different host matrices that can be used to embed the nanoparticles, polymers are of particular interest because of their unique properties. The surfaces of nanoparticles are often modified with specific molecules to impart novel functions such as extended circulation time and specific-targeting [2] and such entities are termed as "stealth particles."

The design and synthesis of magnetic nanocomposites have recently been the focus of intense investigations, particularly because of enhanced properties of such materials. It is known that iron oxide (magnetite, Fe_3O_4; maghemite, Fe_2O_3) nanoparticles acquire superparamagnetism at room temperature if the core diameter of the particle is ~20 nm or less.[3] Superparamagnetic properties depend on the size of FeO : Fe_2O_3 nanoparticles as well as their homogeneous dispersion throughout the polymeric network thus providing a multifunctional avenue for scientific and clinical applications, such as biosensors, protein and cell separation systems and magnetic carriers for hyperthermia and tissue-specific drug delivery.[4] The superparamagnetic particles (SPOINs) can be easily magnetized and localized into a specific area by an external magnetic field, and redispersed once the magnetic field is removed.[5] They can also be expected to facilitate intravenous delivery of drug to the desired site (e.g., tumor site) using an external magnetic field.[6] This approach is called magnetic drug targeting (MDT) and has emerged as a versatile technique to treat complex diseases. By this technique, high concentrations of chemotherapeutic or radiological agents can be achieved near the target site without any toxic effects to normal surrounding tissue.[7]

Iron oxide nanoparticles are highly biocompatible because the iron uptake, transport and storage in the liver are largely regulated by proteins such as ferritin and transferrin.[8] In addition,

Fe-based nanoparticles, such as magnetite (Fe_3O_4) and maghemite (γ-Fe_2O_3), exhibit lower toxicity and less susceptibility to oxidation than other magnetic materials such as cobalt and nickel thus making them suitable for diagnostic and therapeutic strategies.[9] Moreover, surface chemistry and sizes of SPIONs play an essential role in cytotoxicity. Coated SPIONs are known to be significantly less toxic than uncoated ones.[10–12]

In the present study nanocomposites have been prepared by *in situ* synthesis of magnetic nanoparticles within poly(2-hydroxyethyl methacrylate) (PHEMA) based nanoparticles. PHEMA is a well-known biocompatible polymer and has been used in numerous applications such as soft contact lenses, drug delivery systems, kidney dialysis membranes, artificial liver support systems, and nerve guidance channels.[13]

Although various methods have been reported for the synthesis of iron oxide nanoparticles, such as sonochemical synthesis, sol–gel reactions, and chemical solution; however, *in situ* coprecipitation method is normally preferred for homogeneous dispersion of inorganic moieties within a polymer matrix. Srivastava et al.[14] reported the synthesis of superparamagnetic bare Fe_3O_4 nanostructures and core/shell (Fe_3O_4/alginate) nanocomposites by coprecipitation and *in situ* coprecipitation methods, respectively. Rodrigueza et al.[15] prepared magnetite-based nanoparticles precipitated in mesoporous styrene–divinylbenzene microspheres by chemical coprecipitation process. Gyergyek et al.[16] prepared superparamagnetic nanoparticles dispersed in a polymethyl methacrylate matrix having a high loading of magnetic nanoparticles. Perçin et al.[17] reported synthesis of magnetic poly(hydroxyethyl methacrylate-N-methacryloyl-(L)-histidine) (PHEMAH) nanoparticles for plasmid DNA purification from *Escherichia coli* cell lysate.

It is well recognized that the superparamagnetic behavior and allied magnetic properties as well as the performance of nanocomposites greatly depend on how uniformly the magnetic particles are impregnated inside the bulk of the host polymer. Inhomogeneous impregnation of magnetic oxide material is known to cause adverse impacts on both the end-properties and performance of hybrid materials, especially when they are employed for drug delivery purposes. Thus, designing PHEMA nanocarriers embedded with evenly dispersed iron oxide particles motivated the authors to undertake the present research task. In order to achieve this goal a novel approach was adopted for getting biocompatible and uniformly dispersed iron oxide impregnated PHEMA nanocomposites which may further be used as a carrier in MDT approach. The prepared magnetic nanoparticles (magnetic PHEMA (mPHEMA)] were characterized by various analytical techniques viz. Fourier transform infrared spectroscopy (FTIR), X-ray diffraction (XRD) technique, vibrating sample magnetometer (VSM), transmission electron microscopy (TEM), and elemental analysis.

EXPERIMENTAL

2-Hydroxyethyl methacrylate (HEMA; Mw = 130.14, bp = 67°C, d = 1.071, inhibited by MEHQ 200–220 ppm) and ethylene glycol dimethacrylate (EGDMA; Mw = 198.22, d = 1.053, bp = 66°C stabilized with 0.01% hydroquinone monoethyl ether) were purchased from Sigma Aldrich Co. and used as monomer and crosslinker, respectively. Benzoyl peroxide (BPO) (Mw=242.23, mp = 102–105°C) used as the initiator was obtained from Merck (Mumbai, India) and polyvinyl alcohol (PVA) (14,000 kDa, hot process; Merck) was used as stabilizer. Toluene (Merck) was taken as solvent and ferrous chloride and ferric chloride hexahydrate were obtained from Merck. All other chemicals used were of analytical grade, and doubly distilled water was used throughout the experiments.

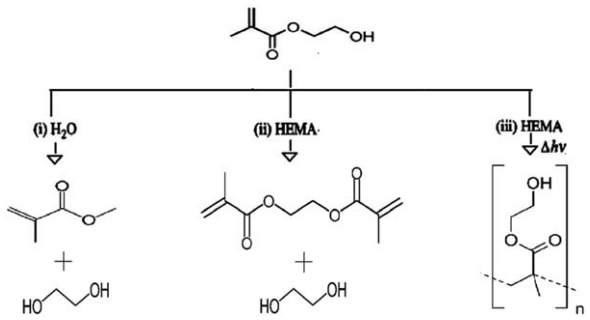

Figure 1. Possible side reactions of HEMA monomer (i) formation of ethylene glycol and methacrylic acid, (ii) transesterificaton of two HEMA molecules to yield EDGMA and ethylene glycol, and (iii) polymerization of HEMA to give PHEMA.

METHODS

Purification of Monomer

The HEMA monomer has quite poor stability due degradation of monomer during transportation and storage at ambient temperatures which may result in increased levels of methacrylic acid (MAA) and the natural occurring crosslinker EGDMA. The high purity of the monomer is essential in synthesis of nanoparticles as omitting impurities greatly improve the physicochemical characteristics of the end polymer. As illustrated in Figure 1, the HEMA monomer readily undergoes the following three common reactions:

(1) Hydrolysis of HEMA at the ester linkage to form MAA and ethylene glycol.

(2) Formation of EGDMA which is also a crosslinker and ethylene glycol can occur by transesterification of two molecules of HEMA.

(3) Polymerization of HEMA at the double bond yields oligomer and polymer.

The purification and evaluation of purity of HEMA monomer was performed by the procedure described by Bajpai and Chouhan.[13] The impurity of MAA in HEMA monomer was removed by stirring the monomer with anhydrous Na_2CO_3 (15%, w/v) for 3 h at 27°C, then vacuum filtering through Whatman filter papers. The EGDMA was removed by first dissolving the above treated monomer in three times its volume of distilled water. Thereafter, four extractions were performed with mixture of carbon-tetrachloride and cyclohexane (50 mL of 1 : 1, v/v, 25 mL each), allowing the layers to separate for 30 min between two extractions. The organic layer containing EGDMA was discarded after each extraction and the aqueous phase was placed under vacuum to remove any remaining organic solvent. The HEMA was then salted out with NaCl (100 g), dried with

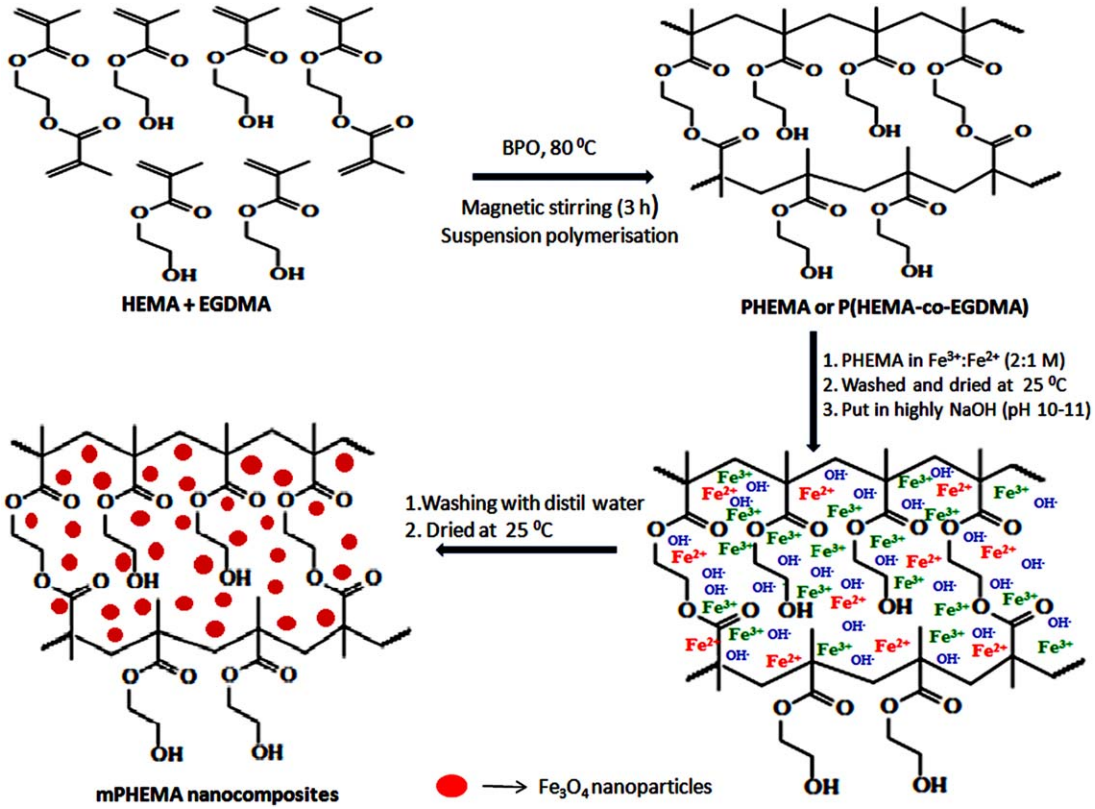

Figure 2. Schematic representations of polymerization of HEMA and subsequent impregnation of iron oxide into the polymer matrix by *in situ* precipitation of iron salts by addition of alkali to yield mPHEMA nanocomposites. [Color figure can be viewed in the online issue, which is available at wileyonlinelibrary.com.]

anhydrous Na_2SO_4, and filtered. The partially purified HEMA monomer was vacuum distilled in the presence of hydroquinone (1 g; added to prevent polymerization) at 60 mmHg and after distillation the pure HEMA was transferred to an opaque glass bottle and stored at 0°C until use.

Purity of HEMA

The purity of distilled HEMA was determined by high-pressure liquid chromatography (HPLC), [Backmen System (Gold 127)] equipped with a ultraviolet (UV) detector, a 25 cm × 46 mm id separation columns ODS (C18), 5 μm particle size. The UV detector was set at 217 nm. The mobile phase was methanol–water (60 : 40, v/v) and the flow rate was kept at 1 mL/min. All samples were diluted with pure methanol to 1/1600. Samples of 10 μL were injected for each analysis. Samples of known concentrations of MAA and EGDMA were injected into the HPLC, and the resultant chromatogram was used to construct a standard curve of known concentrations vs. area under the curve. The chromatogram showed three distinct peaks. The first peak, at 3.598 min was identified as MAA and the next peak at 5.512 min was the major peak due to HEMA monomer. The impurities of MAA and EGDMA in the monomer samples were found to be less than 0.01 mol % MAA and 0.001 mol % EGDMA.

Preparation of Iron Oxide Containing mPHEMA Nanocomposites

Synthesis of mPHEMA nanocomposites involves a two step process in which the first step is the preparation of native PHEMA nanoparticles and in the second step iron oxide is allowed to precipitate *in situ* inside PHEMA nanoparticles matrix to yield mPHEMA nanocomposites.

Preparation of Poly(2-hydroxyethyl methacrylate) Nanoparticles. Poly(2-hydroxyethyl methacrylate) (PHEMA) nanoparticles were prepared by a modified suspension polymerization method. In this method a mixture of monomer HEMA (1 mL, 7.16 mmol) and initiator BPO (60 mg, 0.247 mmol) dispersed in toluene was added into an aqueous phase containing PVA (1.5 g, 0.140 mmol). The reaction mixture was stirred vigorously at 600–700 rpm and while stirring, the crosslinker EGDMA (0.3 mL, 1.4 mmol) was added drop wise into the stable suspension of reaction mixture and kept initially at 80°C for 2 h and then 90°C for 1 h to ensure complete polymerization process. After the crosslinking reaction was completed the reaction mixture was allowed to cool so that the polymeric particles were separated. The nanoparticles were purified by washing them thrice with toluene and twice with acetone. The collected nanoparticles were dried at 25°C for a week to obtain a fine white powder which was further stored in an airtight polyethylene bags.

Incorporation of Iron Oxide in PHEMA Nanoparticles. Iron oxide nanoparticles were synthesized within PHEMA nanoparticle matrix by *in situ* precipitation method. The main advantage of the precipitation process is that a large amount of iron oxide nanoparticles can be synthesized.[18]

In this method, the dried PHEMA nanoparticles were placed in an aqueous solution of mixture of ferrous and ferric salts of molar ratio (1 : 2, 0.5/1 *M*) and allowed to swell for 24 h so that both ferrous and ferric ions were entrapped inside the polymer matrices. Prior to putting them in salt solutions a dry stream of N_2 was flushed for at least 1 h so as to check critical oxidation of the magnetite and reduce the particle size.[19] The swollen nanoparticles were taken out and washed by mildly shaking them several times in distilled water to make them free from unreacted salts and chemicals, and then filtered under vacuum. The swollen nanoparticles were then put into an alkaline solution (10% NaOH) for definite time period so that ferrous and ferric ions get precipitated within the polymer matrix to form magnetite. It is worth to mention here that the size of nanoparticles depends on pH and temperature of the medium. It is known that the higher the pH and ionic strength, the smaller would be the particle size and size distribution width. These parameters are significant as they determine the chemical composition of the crystal surface and consequently the electrostatic surface charge of the nanoparticles.[18]

The formation of iron oxide nanoparticle within the polymer matrix can be shown by the following reaction:

$$2FeCl_3 + FeCl_2 + 8NaOH \rightarrow Fe_3O_4 + 8NaCl + 4H_2O \quad (1)$$

It is essential to create a non oxidizing environment during precipitation for preventing oxidation of precipitated magnetite in highly alkaline medium otherwise their oxidation can favor formation of undesired ferric hydroxide as shown below:

$$Fe_3O_4 + \frac{1}{2}O_2 + \frac{9}{2}H_2O \rightarrow 3Fe(OH)_3 \quad (2)$$

It is well known, that in homogeneous precipitation the reactants are dissolved in the reaction phase before start of the reaction.[20] So, the slow and gradual penetration of OH^- ions into the polymer matrix with respect to time leads to formation of uniform magnetite precipitate in the matrix.

At the end of precipitation, the change in color of nanoparticles from white to creamish-brown confirms the formation of oxides of iron. The prepared iron oxide containing PHEMA nanoparticles (mPHEMA) were again washed several times with distilled water, vacuum filtered, dried at room temperature, and stored in airtight polyethylene bags. The polymerization of PHEMA and subsequent *in situ* precipitation of iron oxide within the polymer matrix is schematically represented in Figure 2. The percentage of impregnation of iron oxide into the nanoparticles can be calculated by the following equation:

$$\text{Impregnation of iron oxide}\,(\%) = \left[\frac{W_{\text{impregnated}} - W_{\text{dry}}}{W_{\text{dry}}}\right] \times 100 \quad (3)$$

where $W_{\text{impregnated}}$ is the weight of dry impregnated nanocomposites and W_{dry} is the initial.[21]

CHARACTERIZATION

FTIR Spectral Analysis

FTIR spectra of native iron oxide nanoparticles, PHEMA nanoparticles and mPHEMA nanocomposites were recorded on a FTIR-8400, Shimadzu Spectrophotometer in the range 400–4000 cm^{-1} with a resolution of 2 cm^{-1}. Samples for spectral analysis were prepared by mixing nanoparticles and KBr in 1 : 10 proportion.

XRD Technique

The XRD studies of nanoparticles were carried out on a Brukker D8 advance XRD powder diffractometer. The diffraction data were collected in the range 10–70, 2θ with a step size of 0·02 and counting time of 2 s $step^{-1}$. The average crystallite size of iron oxide particles was estimated using Debye–Scherer's equation.

Raman Spectral Analysis

Micro Raman system from Jobin Yvon Horibra LABRAM-HR visible (400–1100 nm) was used to obtain Raman spectra, with excitation laser sources of He–Ne 632.8 nm and argon 488 nm. Spectra can be recorded from 50 cm^{-1} to 4000 cm^{-1} of Raman shift.

Energy-Dispersive X-ray Analysis

Energy-dispersive X-ray (EDS or EDX) is an analytical technique used for the elemental analysis or chemical characterization of a sample. In the present study the technique was used to determine elemental percentage composition of prepared material using Philips, Netherlands ESEM EDAX XL-30 instruments.

VSM Analysis

SQUID vibrating sample magnetometer (VSM) was used to study the magnetic properties of native iron oxide and mPHEMA nanocomposites at room temperature. The instrument used was PPMS—VSM workable in the temperature range of 2–350 K and magnetic field up to 140 kOe. The sensitivity was 10–5 emu and temperature stability was 10 mK.

TEM Studies

TEM was performed by using a Philips, Holland Tecnai 20 transmission microscope with magnifications of the order of 750,000 xs. TEM measurements were done by dispersing a drop of the sample suspension on Formvar-coated C grids.

ED Spectroscopy

In order to investigate the crystalline nature of prepared mPHEMA nanocomposites electron diffraction (ED) studies were performed on Philips, Holland Tecnai 20 Transmission Electron Microscope.

Field-Emission Scanning Electron Microscopy

The FE scanning electron microscope (FE-SEM) is normally used to visualize very minute topographic details on the surface or entire or fractioned objects. Nova nanosem 430 IE Synergy 250 (X-Max 50 LN2 Free) was used for analysis having magnification of the order of 8.00 lacs and resolution 1 nm.

Dynamic Light Scattering Measurements

Electrophoretic light scattering (ELS) Beckman Coulter Delso Nano C instrument was used for particles size analysis which determines electrophoretic movements of charged particles under an applied electric field. This instrument is capable of measuring hydrodynamic radii in the range of 1–7000 nm and molecular weight as small as 267 Da in a concentration range of 10 ppm to 40% (w/v).

Table I. Gradation of Cytotoxicity

Grade	Reactivity	Conditions of all cultures
0	None	Discrete intracytoplasmic granules, no cell lysis, no reduction of cell growth
1	Slight	Not more than 20% of the cells are round, loosely attached and without intracytoplasmatic granules, or slow changes in morphology; occasional lysed cells are present; only slight growth inhibition observable
2	Mild	Not more than 50% of the cells are round, devoid of intracytoplasmatic granules, no extensive cell lysis; not more than 50% growth inhibition observable
3	Moderate	Not more than 70% of cell layers contain rounded cells or are lysed; cell layers are not completely destroyed, but more than 50% growth inhibition observable
4	Severe	Nearly complete or complete destruction of cell layers.

Zeta Potential and Electroosmotic Stream Measurements

Zeta potential studies were performed with Beckman Coulter Delso Nano C instrument for analysis of particles size and electrophoretic light scattering (ELS), which determine electrophoretic movement of charged particles under an applied electric field from the Doppler shift of scattered light.

In Vitro Cytotoxicity Test

In order to determine *in vitro* cytotoxicity of the prepared materials, test using test on extract was performed based on (ISO10993-5, 2009). In this method, 0.2 g powdered material was soaked in culture medium (1 mL) with serum and then the extract was prepared by incubating the presoaked test material with serum for 24 h. After incubation, the extract was filtered using 0.22 μm millex gp filter. 100% extract was diluted with culture medium to get 50% and 25% concentrations. Different dilutions of test sample extracts, positive control, and 100% extracts of negative control in triplicate were placed on subconfluent monolayer of L-929 cells. After incubation of cells with extracts of the test sample and controls at 37 ± 1°C for 24–26 h, culture was examined microscopically for cellular response and scored as 0, 1, 2, 3, and 4 based on the following Table I. For negative control, the sample was prepared by incubating 1.25 cm^2 polyethylene discs with 1 mL culture medium with serum at 37 ± 1°C and positive control was prepared by diluting phenol stock solution (13 mg/mL) with culture medium with serum.

RESULTS AND DISCUSSION

Effect of Iron Salts on Iron Oxide Impregnation

In the present study, an *in situ* coprecipitation method was used to design iron oxide impregnated PHEMA nanoparticles as discussed under Methods section. Inclusion of iron oxide into the polymer matrix results from *in situ* precipitation of ferrous/ferric ions when treated with alkaline solution.

In order to study the effect of composition of iron oxide in PHEMA nanoparticles, the mPHEMA nanocomposites containing different iron oxides were prepared by changing oxidation form of iron as well as its molar ratio. In these experiments, the PHEMA nanoparticles were allowed to swell in three different iron salt solutions viz. Fe^{2+} (0.5 *M*), Fe^{3+} (1 *M*), and Fe^{3+}/Fe^{2+} (2 : 1 *M*) which facilitated an entrapment of different types of iron ions into nanoparticles matrix; one containing only Fe^{2+} ions, other only Fe^{3+} ions and one having both Fe^{3+} and Fe^{2+} ions. Afterward, these particles were subjected to precipitation of iron oxide in alkaline medium. Now it can be hypothesized that the PHEMA nanoparticles containing only Fe^{3+} and Fe^{2+} ions lead to the formation of maghemite (γ-Fe_2O_3) and hematite (α-Fe_2O_3) oxides of iron whereas PHEMA nanoparticles having both Fe^{3+} and Fe^{2+} ions in 1 : 2 molar ratio preferred the formation of magnetite (Fe_3O_4).

The mechanistic aspects of iron oxide formation are represented by the following chemical equations. The formation of hematite or maghemite from ferrous ions inside polymer matrix via formation of iron hydroxide may be shown as

$$Fe^{2+} + 2OH^- \rightarrow Fe(OH)_2 \quad (4)$$

In case of oxidation, the ferrous hydroxide formed can also transform into ferric hydroxide. The ferrous and ferric forms of hydroxides lead to the formation of maghemite as shown below:

$$4Fe(OH)_2 + O_2 + 2H_2O \rightarrow 4Fe(OH)_3 \quad (5)$$

$$Fe^{3+} + 3OH^- \rightarrow Fe(OH)_3 \quad (6)$$

$$2Fe(OH)_2 \xrightarrow{\Delta} Fe_2O_3 + 3H_2O \quad (7)$$

$$2Fe(OH)_3 \xrightarrow{\Delta} Fe_2O_3 \quad (8)$$

The synthesis of Fe_2O_3 oxide takes place by dehydration of $Fe(OH)_3$ or $Fe(OH)_2$ from the solution phase and It indicates that the prepared nanoparticles are irregular in shape. The possible mechanism for the formation of plate-like magnetic nanoparticles is ascribed to the slight magnetic dipole-dipole interactions between the magnetic nanoparticles, transforming from $Fe(OH)_3$ or $Fe(OH)_2$ to Fe_2O_3. During this process, however, there happens an anisotropic growth of the nanoparticles which may obviously contribute to magnetic anisotropy property. However, the concentration of $FeCl_2$ or $FeCl_3$ solutions may have little influence on the crystal structure and morphology of the Fe_2O_3 nanoparticles, but can obviously influence the content of the Fe_2O_3 nanoparticles in polymer network as reported in the case of cellulosic films.[22]

While in case of preparation of mPHEMA nanocomposites, Fe_3O_4 nanoparticles are directly formed within the polymeric matrix by treatment of NaOH solution on Fe^{3+}/Fe^{2+} ions, having nearly regular morphology, which is in agreement with the work reported elsewhere.[22] It is also learned that formation of

Table II. Data Showing (%) Impregnation of Iron Oxide Using Iron Salts at Different Oxidation States

S. no.	Fe content	HEMA (mmol)	EGDMA (mmol)	BPO (mmol)	PVA (mmol)	Percent impregnation
1	Fe^{2+} (0.5 *M*)	7.16	1.4	0.247	0.140	6
2	Fe^{2+}/Fe^{3+} (1 : 2)	7.16	1.4	0.247	0.140	9
3	Fe^{3+}(1 *M*)	7.16	1.4	0.247	0.140	7.1

magnetite in oxidation free environment ensures almost no possibility of its conversion into any other forms because the major product of magnetite is maghemite which requires high temperature for transformation as shown below:

$$Fe_3O_4 \xrightarrow{200^{\circ}C} \gamma Fe_2O_3 \quad (9)$$

The magnetite in solution oxidizes very slowly to maghemite, at room temperature over a period of several months.[23] With the concern of getting an appreciable amount of iron oxide impregnation in the polymeric nanoparticle matrix, percentage impregnation of iron oxide in all the three varieties of mPHEMA nanocomposites was observed by the procedure discussed in methodology using eq. (3).[21] It was found that mPHEMA nanocomposites with pure magnetite content showed the highest percentage of impregnation as shown in Table II. Moreover, the homogeneous dispersion of magnetic nanoparticles (Fe_3O_4) obtained via *in situ* coprecipitation method enhanced the extent of percent incorporation of magnetite within the matrix which leads to high and uniform magnetic properties. This may be due to availability of sufficient amount of ferrous and ferric ions in order to precipitate magnetite whereas samples having ferrous and ferric alone showed relatively lower degree of impregnation in PHEMA matrix. This observation can also be correlated with the equilibrium swelling behavior of all the three iron oxide loaded samples.

It is interesting to note that the γ-Fe_2O_3 ultrafine superparamagnetic iron oxide shows a fair cellular uptake in serum medium and cause the induction of DNA damage which results in the cell death and ROS production in endothelial cells, while Fe_3O_4 nanoparticles have been reported for fair biocompatibility and lack of toxicity.[24]

During the synthesis of ultra fine SPIONs and their subsequent environmental oxidation/reduction reactions, the composition with respect to the oxidation state of iron can vary considerably

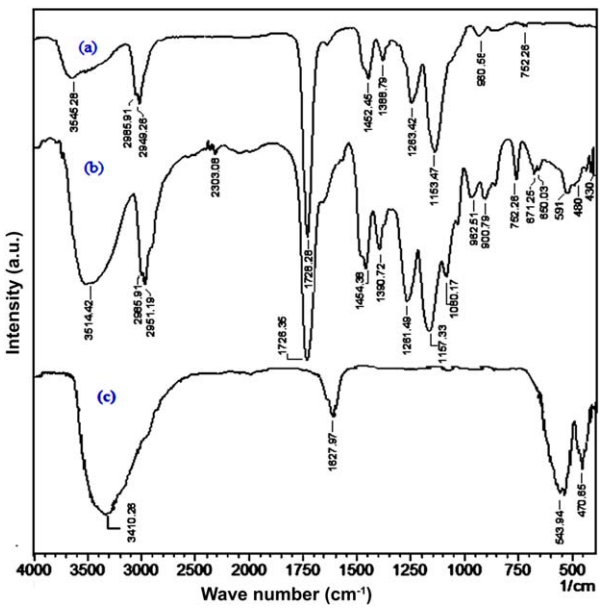

Figure 3. FTIR spectra of (a) PHEMA nanoparticles, (b) mPHEMA nanocomposites, and (c) native iron oxide nanoparticles. [Color figure can be viewed in the online issue, which is available at wileyonlinelibrary.com.]

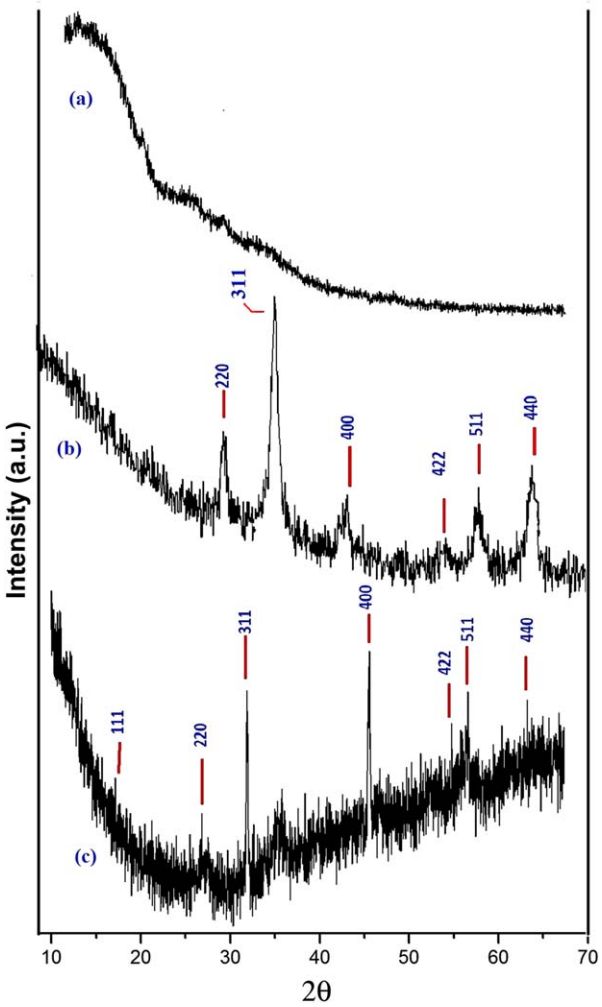

Figure 4. XRD spectra of (a) PHEMA, (b) mPHEMA, and (c) iron oxide nanoparticles (magnetite). [Color figure can be viewed in the online issue, which is available at wileyonlinelibrary.com.]

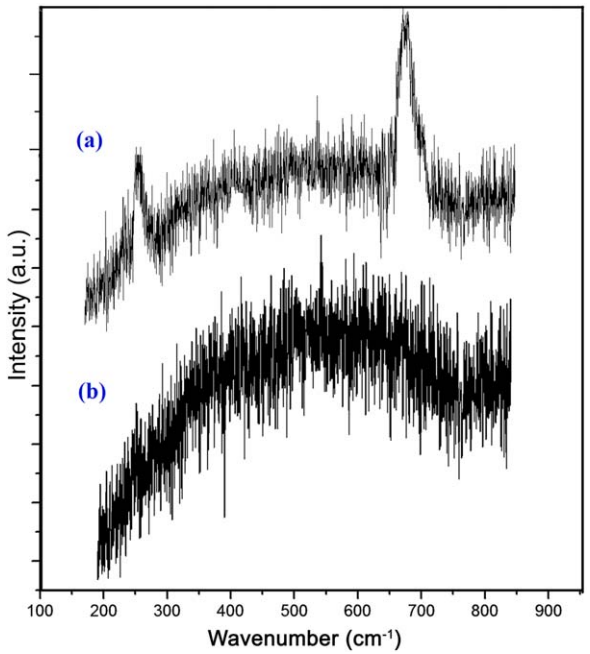

Figure 5. Raman spectra of (a) PHEMA nanoparticles and (b) mPHEMA nanocomposites. [Color figure can be viewed in the online issue, which is available at wileyonlinelibrary.com.]

across the solid solution range of Fe_3O_4 to γ-Fe_2O_3.[25] With an aim of getting nontoxic and highly magnetizable SPOINs encapsulated within PHEMA matrix, a strict check was kept in oxidation state of iron in mPHEMA nanocomposites.

Physicochemical Characterization

Fourier Transformation-Infrared Spectroscopic Analysis. The FTIR spectra of PHEMA nanoparticles and mPHEMA nanocomposites are shown in Figure 3 which clearly marks the presence of HEMA as evident from the appearance of broad absorption peak in the range 3600–3410 cm^{-1} due to hydrogen bonded OH groups of the PHEMA macromolecule. The characteristic carbonyl bond (C═O stretching) also appears at 1728 cm^{-1} and confirms the presence of HEMA in the PHEMA nanoparticles. The other observed peaks are seen at 1261 cm^{-1} (CO stretching vibration), 1157 cm^{-1} (O–C–C stretching), 2962 cm^{-1} (C–H stretching of CH, CH_2, and CH_3 groups) 1280 and 1390 cm^{-1} (twisting and wagging vibrations of methylene group), 1452 cm^{-1} (OH bending), 1080 cm^{-1} (from C–O stretching), 962 and 900 cm^{-1} (C–H oop bending), respectively.

Furthermore, the FTIR spectra of mPHEMA nanocomposite also show all the significant absorption bands of PHEMA along with some characteristic bands of iron oxide. Magnetite form of iron oxide is exhibited in the low frequency region (600–400 cm^{-1}) due to the iron oxide structure. Iron oxide, Fe_3O_4, has inverse type spinel structure that exhibits mainly two absorption bands at 600 and 400 cm^{-1} corresponding to the metal–oxygen bond in tetrahedral and octahedral sites, respectively.[26] The spectral peaks at 591 cm^{-1}, 480 cm^{-1}, and 430 cm^{-1} may be attributed to the Fe–O bonds depending upon the iron content in magnetite (Fe_3O_4). A slight broadening of the band at 591 cm^{-1} may be attributed to the formation of reduced size particles of magnetite (20–30 nm).[27]

By comparing the FTIR spectra of iron oxide [Figure 3(c)], native PHEMA nanoparticles [Figure 3(b)], and mPHEMA nanocomposites [Figure 3(a)], it is clear that iron oxide is embedded as magnetite in the polymer matrix. Moreover, there is no shifting of the spectral peaks of mPHEMA which suggests that Fe–O–Fe inorganic network does not have any chemical bonding with the organic PHEMA matrix thus confirming the successful *in situ* coprecipitation of iron oxide within the polymeric matrix.

XRD Analysis. The XRD was used to study the crystalline properties of iron oxide in mPHEMA nanocomposite and it revealed characteristic peak of native magnetic Fe_3O_4. The XRD patterns of the PHEMA nanoparticles, native Fe_3O_4 nanoparticles and mPHEMA nanocomposites are shown in Figure 4(a–c), respectively. In the spectra of PHEMA [Figure 4(a)], no characteristic diffraction peak is observed which suggests for the amorphous nature of polymer matrix. The XRD diffractrogram of native Fe_3O_4 [Figure 4(c)] with sharp peaks at 111, 220, 311, 400, 422, 511, and 440 may be attributed to magnetite Fe_3O_4, based on the standard JCPDS data (74–748). Comparing to single phase Fe_3O_4 nanoparticles, the mPHEMA nanocomposites [Figure 4(c)] suggested the formation of highly nanocrystalline magnetite with homogenous embedding in polymer matrix indexing to the cubic and inverse type spinel. The broadened peaks were observed at 220, 311, 400, 422, 511, and 440 due to the small size of crystallites magnetite content. The disappearance of 111 peak in diffraction pattern of mPHEMA is due to covering of magnetite crystallite by amorphous polymer.[28]

The crystal size was calculated from the line broadening of the XRD pattern using the Scherer formula as given below:

$$d = \frac{k\lambda}{\beta\cos\theta} \tag{10}$$

where d is mean grain size, k is the shape factor, and β is line broadening measured at half-height and expressed in units of 2θ. The amorphous and crystalline nature of the iron oxide present in PHEMA nanoparticles was determined by percentage of crystallinity calculated as below:

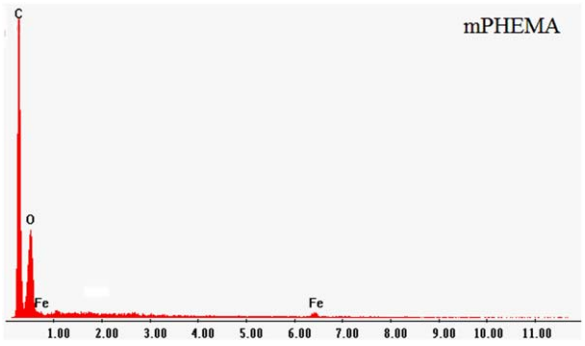

Figure 6. Energy-dispersive spectral spot analyses of mPHEMA nanocomposites. [Color figure can be viewed in the online issue, which is available at wileyonlinelibrary.com.]

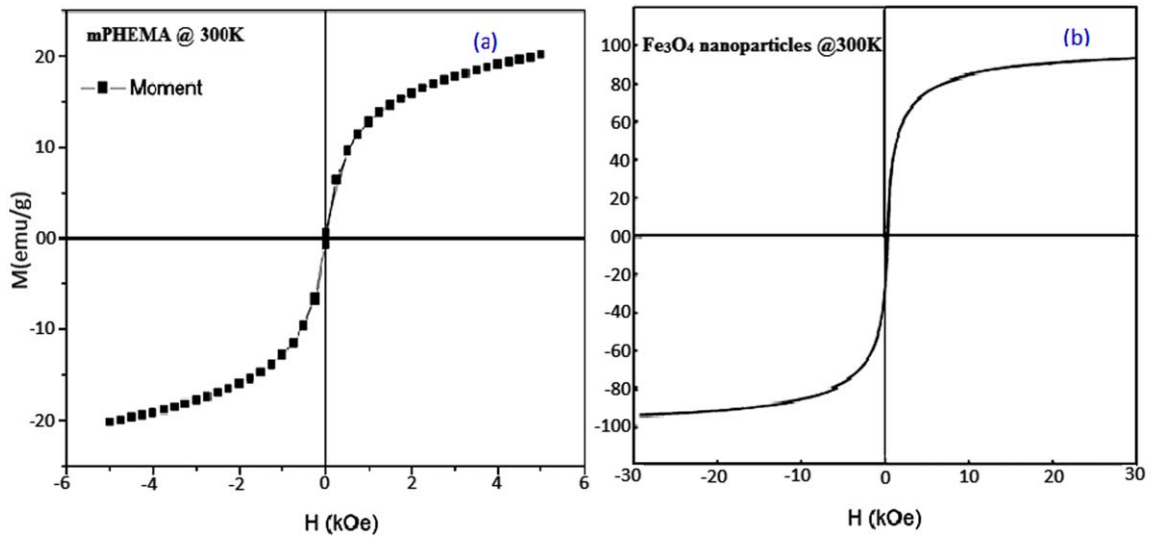

Figure 7. SQUID-VSM of (a) mPHEMA nanocomposites and (b) native Fe_3O_4 nanoparticles at 300 K. [Color figure can be viewed in the online issue, which is available at wileyonlinelibrary.com.]

$$\text{Xc}\ (\%) = \left[\frac{\text{Ac}}{\text{Aa}+\text{Ac}}\right] \times 100 \qquad (11)$$

where Ac and Aa are the area of crystalline and amorphous phases, respectively.

In the present work, for magnetite $\kappa = 0.89$ and $\lambda = 1.54056$ Å for magnetite. The average particle size of Fe_3O_4 in the mPHEMA for the 311 peak was calculated to be 39.1 nm with nearly 92.4% crystallinity. The crystallinity imparted to matrix is mainly due to iron oxide content. Similar type of results were obtained by Prabhakaran and Hemalatha[29] who reported that the inclusion of nano-Fe_3O_4 into the poly(vinylidine fluoride) (PVDF) significantly enhanced the crystallinity of PVDF.

The XRD diffractogram can be supported by the ED pattern obtained for mPHEMA nanocomposites. It is also clear that the spectral intensity of the diffraction peak of iron oxide in the composite is found to be smaller because of lesser amount of iron oxide nanoparticle in the composite material as compared to the bulk magnetite nanoparticles.

Raman Spectral Analysis

The Raman spectral analysis is a valuable tool to derive direct information at the molecular level of the nature of the chemical bonds and symmetry of the material under investigation. In addition, Raman spectroscopy has also been employed to further determine the nature of oxide cores.[30] For correct assignment of the band positions present in the sample and for phase identification, the combined Raman data for key iron oxides bands as given below were used[31]:

Fe_3O_4: 193 (weak), 306 (weak), 538 (weak), 668 (strong);
γ-Fe_2O_3: 350 (strong), 500 (strong), 700 (strong); and
α-Fe_2O_3: 225 (strong), 247 (weak), 299 (strong), 412 (strong), 497 (weak), 613 (medium).

The Raman spectrum corresponding to the samples are shown in Figure 5. The spectra of PHEMA nanoparticles showed no specific absorption bands in the range of 100–800 cm^{-1} and it was taken as base to which that of mPHEMA nanocomposites was compared. The observed spectra [Figure 5(a)] contained the Raman bands corresponding to Fe_3O_4 while mPHEMA nanocomposite showed two new strong broad Raman active bands near 210 cm^{-1} and 675 cm^{-1} due to magnetite.

The spectra corresponding to PHEMA nanoparticles [Figure 5(b)] and mPHEMA nanocomposites do not indicate presence of any interactions between the iron oxide nanoparticles and

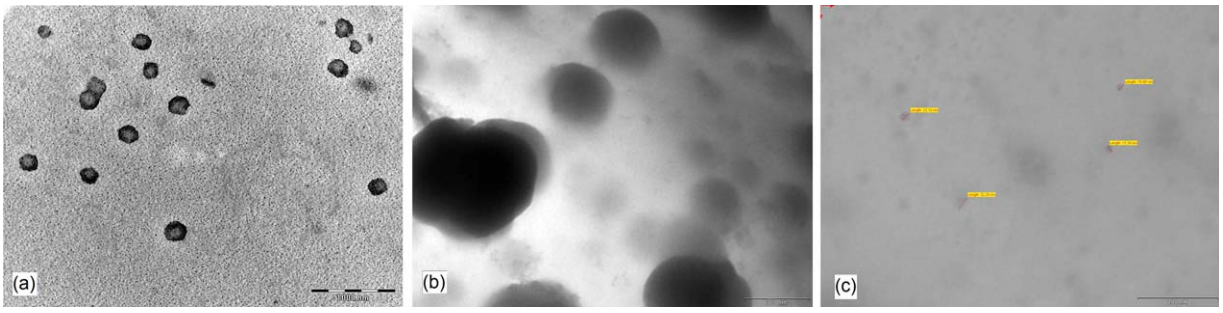

Figure 8. TEM images of (a) PHEMA nanoparticles, (b) mPHEMA nanocomposites, and (c) mPHEMA showing iron oxide nanoparticles (at high magnification). [Color figure can be viewed in the online issue, which is available at wileyonlinelibrary.com.]

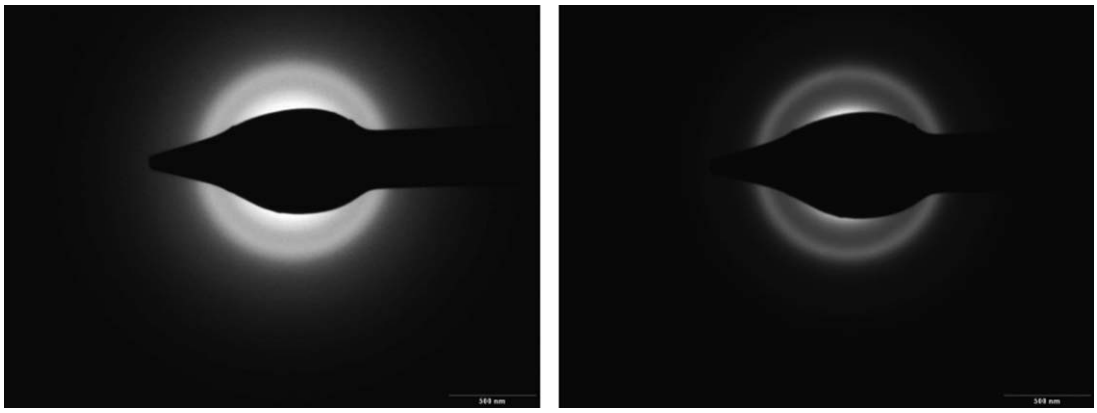

Figure 9. Electron diffraction patterns of mPHEMA nanocomposites.

the polymer matrix and it also confirms that the nanoparticles core is exclusively composed of Fe_3O_4. Almost similar type of results were observed in semi interpenetrating polymer networks (semi-IPNs) of linear alginate and crosslinked poly(N-isopropylacrylamide) (PNiPAAm).[32]

EDX Analysis. In order to determine the percentage of iron content in mPHEMA nanoparticles, EDX analysis was performed. Figure 6 shows the EDX patterns taken simultaneously at two characteristic areas (two spots) of mPHEMA nanocomposites. The analysis revealed that the iron oxide was successfully precipitated within polymer matrix of PHEMA via *in situ* coprecipitation method and the nanocomposite had appreciable iron content (weight percentage) of 0.83% at both spots. The two spot analyses also confirmed the uniform distribution of iron oxide in polymeric matrix. The weight percentage of oxygen and carbon were found to be 29.92% and 69.25%, respectively.

SQUID-Vibratory Sample Magnetometry Studies. To explore the magnetic behavior of the prepared nanocomposites, variation in magnetic moments of iron oxide nanoparticles and their polymer composites was investigated as a function of varying magnetic field.

It is known that magnetite nanoparticles show a spontaneous magnetization than other forms of oxide. Magnetite structure is an inverse spinel with a face centre cubic unit based on $32O^{2-}$ ions with a regularly cubic close packed along the [111] direction. There are eight formula units per unit cell. Magnetite differs from other iron oxides in that it contains both divalent and trivalent iron and its formula may be written as Fe III [Fe II Fe III] O_4 where the brackets denote octahedral sites. Tetrahedral Fe spins are directed antiparallel to octahedral Fe^{3+} and Fe^{2+} spins so that the Fe^{3+} moments are cancelled, leaving a spontaneous magnetization equivalent to one Fe^{2+} moment per molecule. Eight tetrahedral sites are occupied by trivalent iron, and the divalent and trivalent cations occupy the sixteen octahedral sites.[27]

The M–H curve for the magnetic moment of mPHEMA nanocomposites was measured over the range of applied field between −5000 Oe and +5000 Oe at 300 K with a sensitivity of 0.1 emu g^{-1}, whereas the Fe_3O_4 nanoparticles were analyzed at quite higher magnetic field of −30,000–30,000 Oe. The results are shown in Figure 7 which displays a typical S-type curve for mPHEMA nanoparticles. It is also observed that for both Fe_3O_4 nanoparticles and mPHEMA nanocomposites the magnetization decreases from the plateau value and tends to reach zero as magnetic field is gradually removed. This clearly indicates that they have neither coercivity nor remnant magnetization and thus proves their superparamagnetic nature. The reason for superparamagnetic nature of the nanoparticles is essentially due

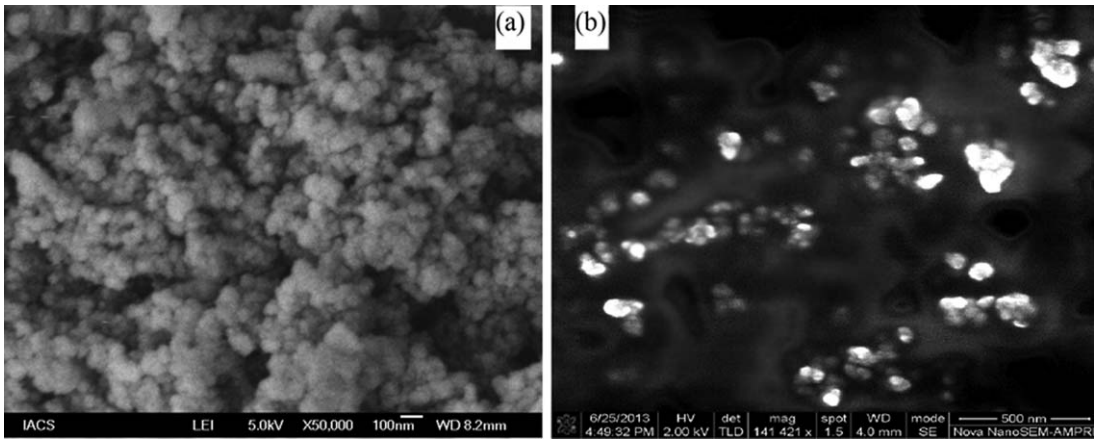

Figure 10. FE-SEM of (a) PHEMA nanoparticles and (b) mPHEMA nanocomposites.

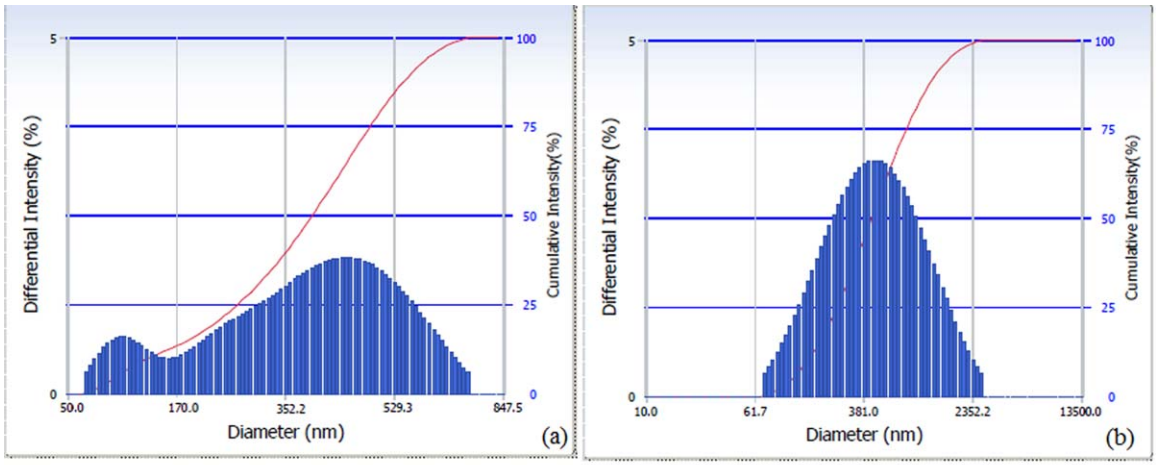

Figure 11. DLS measurements of (a) PHEMA nanoparticles and (b) mPHEMA nanocomposites. [Color figure can be viewed in the online issue, which is available at wileyonlinelibrary.com.]

to very small size of incorporated iron oxide particles which favors the redispersion of magnetic nanoparticles after the external magnetic field is removed. Maghemite, Fe_2O_3, or magnetite, Fe_3O_4 particles having diameter about 10–20 nm are known to show single domains.[33]

The magnetite nanoparticles [Figure 7(b)] possess a very high saturation magnetization of 92 emu g^{-1} as compared to iron oxide containing mPHEMA nanocomposites [Figure 7(a)]. This significant difference in magnetization may be attributed to the reduced particle size of iron oxide within polymer matrix and

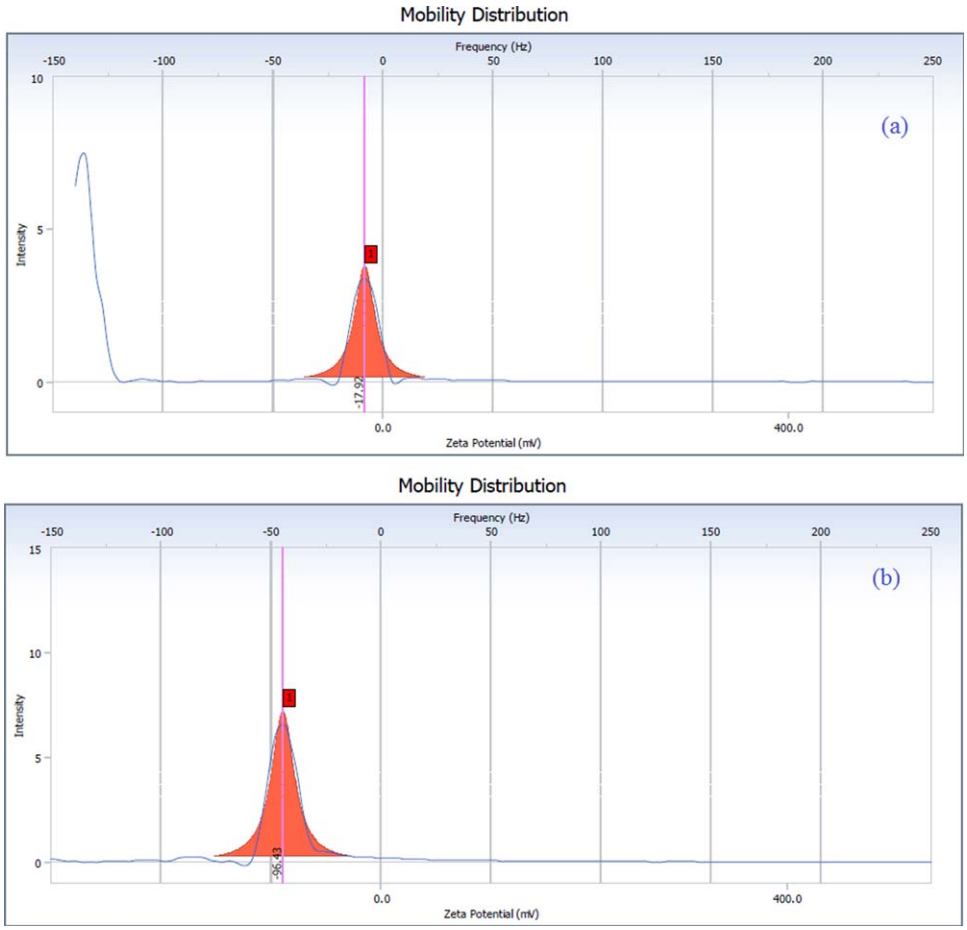

Figure 12. Zeta potential measurements (a) PHEMA nanoparticles and (b) mPHEMA nanocomposites. [Color figure can be viewed in the online issue, which is available at wileyonlinelibrary.com.]

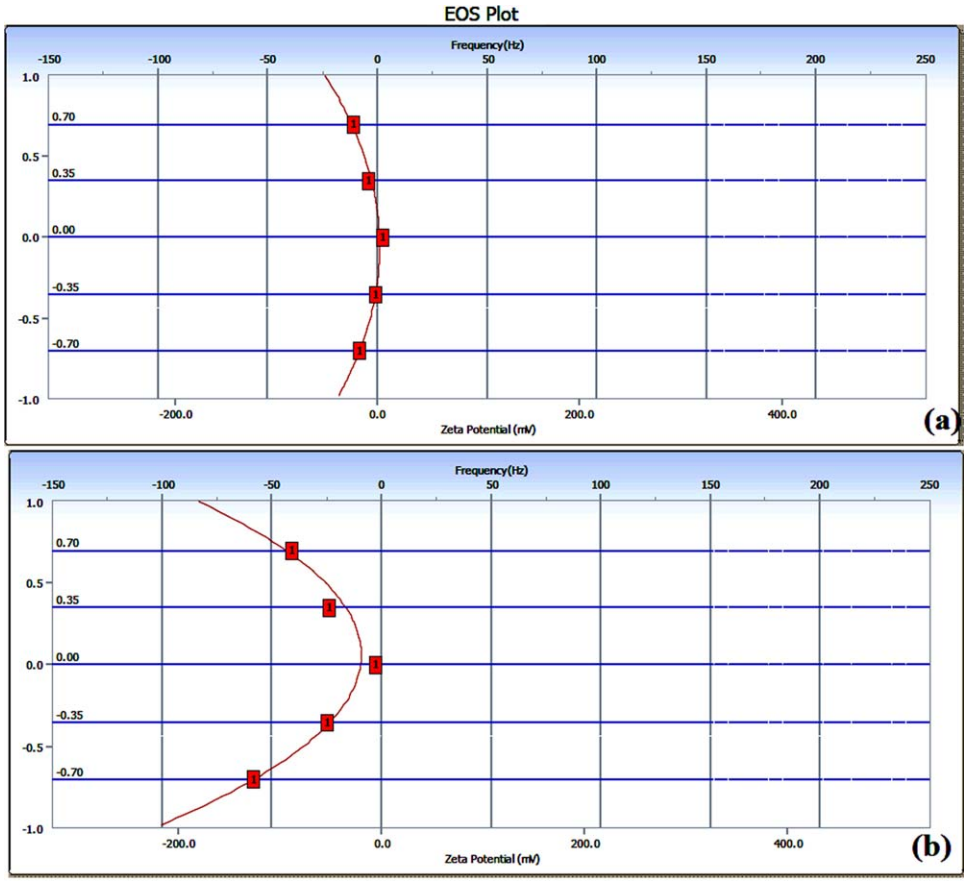

Figure 13. Electroosmotic streaming curve of (a) PHEMA nanoparticles and (b) mPHEMA nanocomposites. [Color figure can be viewed in the online issue, which is available at wileyonlinelibrary.com.]

the concomitant increase in surface area. Casillas et al.[27] explained that saturation magnetization increases when the particle sizes are larger. The decreased Ms value can also be due to diamagnetic nature of PHEMA that shields the Fe_3O_4 nanoparticles, similarly, as in the case of polyacrlyamide hydrogel magnetite nanocomposites (HMNC). The results of low-saturation magnetization in HMNC are attributed to the diamagnetic contribution of the PAM hydrogel matrix covering the Fe_3O_4 nanoparticles.[34] Perçin et al.[17] reported the saturation magnetization value of mPHEMAH nanoparticles about 23.3 emu g^{-1}. Srivastava et al.[14] explained that the smaller size may be considered as equivalent to a single magnetic domain where the energy barrier for its spin reversal is easily overcome by thermal vibrations resulting superparamagnetic nature of nanosize particles. All amorphous nanosized materials show no hysteresis, and the magnetization does not saturate even at 1.5 kOe because of no magnetic content therefore they usually behaves like diamagnetic materials.[35]

TEM Studies. TEM provides a powerful technique to determine size and morphology of the nanoparticles. The size of particles usually refers to the total diameter of the particles and is a key

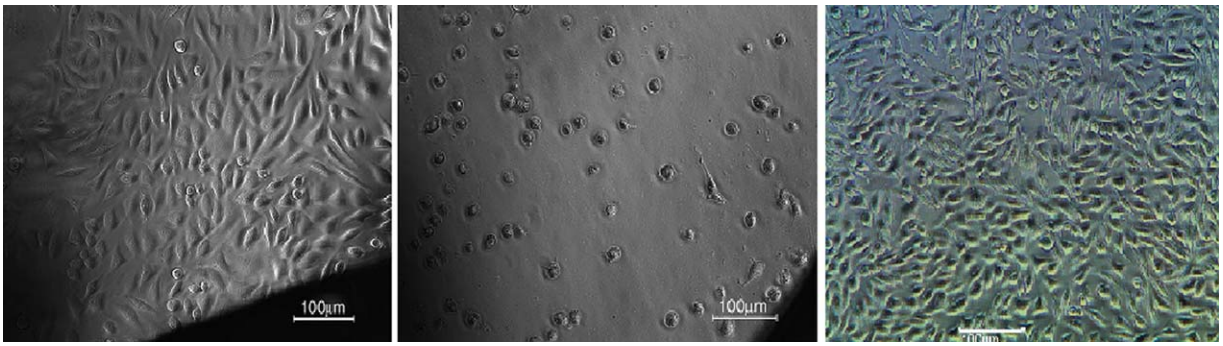

Figure 14. Microscopic images for *in vitro* cytotoxicity showing L-929 cells around (a) positive control, (b) negative control, and (c) mPHEMA nanocomposites. [Color figure can be viewed in the online issue, which is available at wileyonlinelibrary.com.]

property to decide the suitability of the carrier to *in vivo* applications. Since the smallest diameter of capillaries in the body is 4000 nm, larger particles will be mainly captured and withheld in the lungs. Particles with larger sizes and/or aggregation of smaller particles thus may be trapped, causing emboli within the capillaries of the lungs.[36]

A TEM analysis of native PHEMA particles [Figure 8(a)] revealed that the particles have uneven but spherical morphology having size in the range of 100–200 nm. On comparing the TEM image of mPHEMA nanocomposites [Figure 8(b,c)] with that of PHEMA nanoparticles, it is clear that mPHEMA nanocomposites build up a core–shell type structure comprising of homogenous core of magnetite surrounded by PHEMA as enveloping shell. The high resolution TEM images of mPHEMA nanocomposites [Figure 8(c)] also confirm the presence of iron oxide nanoparticles in the polymer matrix.

A minute examination of the image also reveals that aggregated mPHEMA nanocomposite shows a smooth surface morphology and the size varies in the range of 200–400 nm. It also reflects from the image that the dark appearance is due to iron oxide nanoparticles as the core of the nanoparticles matrix. Core/shell structure (magnetite/PHEMA) appearing in the TEM image shows concentrated core and lighter shell well dispersed in the whole matrix of nanoparticles. This also reveals that the *in situ* formation of magnetic nanoparticles was homogeneous, and there was no agglomeration during precipitation of the magnetite nanoparticles.[37] It is always desirable to achieve a more uniform size distribution which results in a narrow magnetization distribution thus ensuring a reproducible magnetic response.[38] Similar type of results were also reported by Yang et al.[39] in which magnetite nanoparticles were uniformly encapsulated as core within the ε-caprolactone nanoparticles. Moreover, recently Arious et al.[40] reported colloidal composite particles consisting of a magnetite core and a biodegradable polymeric shell of poly(ethylene-2-cynoacryltae) by anionic polymerization.

ED Studies. The ED pattern of mPHEMA nanocomposites exhibits continuous concentric rings suggesting for the random polycrystalline structure of iron oxide with weaker intensity due to enveloping of iron oxide inside the amorphous PHEMA matrix. The concentric rings at 220 and 311 positions in ED pattern showed that sample has an inverse cubic spinel structure. These positioning of the rings corresponds to the crystalline structure of magnetite as observed by Starodoubtsev et al.[41] The displayed ED pattern in Figure 9 is in a good agreement with the XRD results, confirming the presence of magnetite (Fe_3O_4). The obtained ring pattern shows that there are no additional reflexes (rings) in the ED pattern which rules out the possibility of formation of other forms of iron oxide.

Field-Emission Scanning Electron Microscopy Studies. FE-SEM can yield valuable information regarding the purity of a nanoparticle sample as well as an insight on their degree of aggregation. Moreover, when nanoparticles are part of secondary and tertiary nanostructures, SEM becomes a valuable tool to assess their location.[42] The SEM pictographs are shown in Figure 10(a,b) which clearly suggest that both PHEMA nanoparticles [Figure 10(a)] and mPHEMA nanocomposites [Figure 10(b)] are present as aggregates having nearly spherical shape. The SEM micrograph of PHEMA shows the formation of a heterogeneous surface corresponding to conglomerates of spherical particles and their aggregates. In this case, the network displays a typical example of a polymer bead obtained by suspension polymerization, which looks like a cauliflower.[43] It is also observed that degree of aggregation is small in mPHEMA nanocomposites in comparison to PHEMA nanoparticles with nonuniform size distribution in the range 50–400 nm. In case of mPHEMA nanocomposites a darker shade is expected due to impregnated iron oxide.

Dynamic Light Scattering Studies. Particle size and size distribution are important characteristics of nanoparticle systems as they determine biological fate, toxicity, targeting ability, drug loading, drug release and stability of nanoparticles. The interaction of nanoparticles with living systems depends on their characteristic dimensions.[44] The average particle size was an average of minimum 30 measurements, and the size distribution was recorded automatically by the software.[18] The particle size distribution plot of dynamic light scattering (DLS) is shown in Figure 10 which indicates that the mPHEMA nanocomposites [Figure 11(b)] has the moderate size distribution with a polydispersity index of 0.366. It is reported that PDI values greater than 0.7 indicate that the sample has a very broad size distribution.[45] The small polydispersity index suggests that nucleation is fast as compared to particle growth, and also that the secondary nucleation step is absent.[20] The average size (diameter, nm) of mPHEMA nanocomposites is 605.6 nm, which confirm that the prepared nanoparticles composite lies in the nanometer range whereas in case of PHEMA nanoparticles [Figure 11(a)] it is shown that they are quite lower in size than mPHEMA nanocomposites. This is in good agreement with TEM size analysis which revealed cleared that impregnation of filler has increased the nanocomposites size.

Zeta Potential Studies. The surface chemistry is especially important to avoid the action of the reticuloendothelial system (RES), which is part of the immune system, and increases the half-life in the blood stream.[46] Neutral or hydrophilic surface of nanocarriers can increase the circulatory half-life from minutes to hours or even days. The surface charge plays an important role during endocytosis. There should be a slower uptake for negatively charged particles due to the negative rejection effect of the negatively charged cell membranes. However, the endocytosis index *in vitro* is minimal with a zeta potential close to zero.[47]

The ξ-potential is an important characteristic that determines particle stability. The zeta potential indicates the degree of repulsion between similarly charged particles in dispersion and the resistance to aggregation.[45] The colloidal stability of the prepared nanocomposites was evaluated from the distribution of zeta potential and profile of the electroosmotic stream (EOS) plot concerning electrokinetic potential in the colloidal dispersions as shown in Figures 12 and 13, respectively. Figure 12 shows zeta potential curve of PHEMA nanoparticles [Figure 12(a)] and mPHEMA nanocomposites [Figure 12(b)], respectively.

Considering PHEMA is a neutral polymer, the mobility distribution curve and EOS plot of native PHEMA nanoparticles had

a zeta potential of −17.92 mV. Most of the polymeric materials have a negative surface charge even if they do not have any negatively charged groups. In fact, surface ξ-potentials of poly(ethylene terephthalate) and poly(butyl methacrylate) [pBMA] are −41 mV and −36 mV, respectively. The hydrated polymer, poly(HEMA) also has a negative ξ-potential, of −16 mV.[48] The slight negative charge may arise from deprotonation of hydroxyl groups of HEMA. The mPHEMA nanocomposites showed a quite higher zeta potential of −96.43 mV. The EOS plots of PHEMA nanoparticles [Figure 13(a)] and mPHEMA nanocomposites [Figure 13(b)] obtained were parabolic in shape which indicates that these particles can be considered to be fairly dispersed in the medium taken. This increase in the surface potential may be explained by the presence of iron oxide in the polymeric matrix as anionic form (FeO^-) of iron oxide. The electrokinetic potential of HEMA was also net negative. The increase in zeta potential of PHEMA was also observed when the HEMA polymer films incorporated with MMA units with an increasing amount of bulk charge.[49]

***In Vitro* Cytotoxicity Test.** The cytocompatibility of mPHEMA nanocomposites was judged by *in vitro* cytotoxicity test as performed on L-929 fibroblast by extract method. The cytotoxicity reactivity of test and control samples was evaluated under an inverted phase contrast microscope to Grades 0, 1, 2, 3, and 4 as shown in Figure 14. As per ISO 10993-5, the numerical grade greater than 2 is considered as cytotoxic. The negative control was graded 0 showing no reactivity while positive control displayed severe reactivity with Grade 4 as shown in Figure 14(a,b), respectively. The test sample, i.e., mPHEMA nanocomposites exhibited no reactivity with Grade 0 on L-929 fibroblast cells which implies that the condition of culture is having discrete intracytoplasmic granules, no cell lysis, and no reduction of cell growth as shown in Figure 14(c). This proves the biocompatible nature of mPHEMA nanocomposites. The HEMA and itaconic acid P(HEMA/IA) hydrogels copolymer are also reported to have shown better cell viability than native PHEMA, which indicates that the incorporation of itaconic acid improves the cytocompatibility of the hydrogels[50] which can be correlated with the noncytotoxic nature of mPHEMA nanocomposites due to the presence of magnetite content.

CONCLUSIONS

In the present work initially PHEMA nanoparticles were synthesized by free radical suspension polymerization method and subsequently iron oxide was precipitated *in situ* by treating divalent and trivalent irons embedded from the respective hydrated salts solutions in molar ratio (Fe^{2+}/Fe^{3+}) of 1 : 2 with an alkali. This approach resulted in formation of novel nanocomposites with appreciable iron oxide content in the PHEMA nanoparticles matrix. The major focus was to produce mPHEMA nanocomposites having magnetite form of iron oxide due to its better biocompatibility and lower toxicity than other forms of iron oxides such as hematite or maghemite.

In the study, both PHEMA nanoparticles and mPHEMA nanocomposites were characterized physicochemically to judge the enhancement in properties of mPHEMA nanocomposites by incorporation of iron oxide as filler in the matrix. The iron oxide formed *in situ* showed superparamagnetism due to small particle size which was judged by SQUID VSM, which is a significant property for biomedical applications especially in magnetically targeted drug delivery. Various techniques like FTIR, XRD, Raman spectroscopy, and zeta potential were used for the characterization of prepared nanocomposites. TEM, FE-SEM and DLS measurements proved the nanosize of mPHEMA nanocomposites. *In vitro* cytotoxicity test confirms the *cyto*-friendly nature of prepared nanocomposites with zero cytotoxic effect on L-929 fibroblast cells. Thus, it can be concluded that new biocompatible superparamagnetic nanocomposites have been designed as potential nanovehicle which can be used especially in magnetic driven drug delivery.

ACKNOWLEDGMENTS

The authors gratefully acknowledge the financial support provided by Board of Research in Nuclear Sciences, BARC, Trombay, India, in the form of Major research project (No. 2011/53/37C/BRNS/2265). The authors would also like to acknowledge UGC-DAE Consortium for Scientific Research, Indore, Madhya Pradesh, India, Institute of Science and Education Research (IISER), Bhopal, India, and Sophisticated Instrumentation Centre for Applied Research & Testing (SICART), Vallabh Vidya Nagar, Gujarat, India, for providing analytical support to carry out physiochemical characterizations of prepared nanoparticles.

REFERENCES

1. Ajayan, P. M.; Schadler L. S.; Braun P. V. Nanocomposites Science & Technology; Wiley-VCH Verlag GmbH Co. KGaA: Weinheim, **2003**. ISBN 3–527-303559-6.
2. Basu, A.; Malakar J. *Elixir International J., Pharmacy.* **2013**, *54*, 12266.
3. Rosena, J. E.; Chana L.; Shieh, D. B.; Gu, F. X. *Nanomed. Nanotechnol. Biol. Med.* **2012**, *8*, 275.
4. Gao, J.; Gu, H.; Xu, B. *Acc. Chem. Res.* **2009**, *42*, 1097.
5. Morrish, A. H. The Physical Principles of Magnetism; IEEE Press: New York, **2001**.
6. Ito, A.; Shinkai M.; Honda, H.; Kobayashi, T. *J. Biosci. Bioeng.* **2005**, *100*, 1.
7. Lokwani, P. *Int. J. Res. Pharm. Biomed. Sci.* **2011**, *2*, 465.
8. Corchero, J. L.; Villaverde, A. *Trends Biotechnol.* **2009**, *27*, 468.
9. Sanvicens, N.; Marco, M. P. *Trends Biotechnol.* **2008**, *26*, 425.
10. Voinov, M. A., Pagan, J. O. S.; Morrison, E.; Smirnova, T. I.; Smirnov, A. *J. Am. Chem. Soc.* **2011**, *133*, 35.
11. Lewinski, N.; Colvin, V.; Drezek, R. *Small* **2008**, *4*, 26.
12. Auffan, M.; Achouak, W.; Rose, J.; Roncato, M. A.; Chaneac, C.; Waite, D. T.; Masion, A.; Woicik, J. C.; Wiesner, M. R.; Bottero, J. Y. *Environ. Sci. Technol.* **2008**, *42*, 6730.
13. Chouhan, R.; Bajpai, A. K. *J. Mater. Sci.: Mater. Med.* **2009**, *20*, 1103.
14. Srivastava, M.; Singh, J.; Yashpal, M.; Gupta, D. K.; Mishra, R. K.; Tripathi, S.; Ojha, A. K. *Carbohydr. Polym.* **2012**, *89*, 821.

15. Rodrigueza, A. F. R.; Coaquira, A. H.; Morales, M. A.; Faria, F. S. E. D. V.; Cunha, R. M.; Santos, J. G.; Silveir, L. B.; Candel, D. R. S.; Baggio-Saitovitch, E. M.; Rabelo, D.; Azevedo, R. B.; Morais, P. C. *Spectrochim. Acta Part A* **2013**, *100*, 101.
16. Gyergyeka, S.; Huskić, M.; Makoveca, D.; Drofenik, M. *Colloids and Surfaces A: Physicochem. Eng. Aspects.* **2008**, *317*, 49.
17. Perçin, I.; Karakoç, V.; Akgöl, S.; Aksöz, E.; Denizli, A. *Mater. Sci. Eng. C* **2012**, *32*, 1133.
18. Mohapatra, M.; Anand, S. *Int. J. Eng. Sci.* **2010**, *2*, 127.
19. Kim, D. K.; Zhang, Y.; Voit, W.; Rao, K. V.; Muhammed, M. *J. Magn. Magn. Mater.* **2001**, *225*, 30.
20. Bakardjieva, S.; Štengl, V.; Šubrt, J.; Večerníková, E. *Solid State Sci.* **2005**, *7*, 367.
21. Gupta, R.; Bajpai, A. K. *J. Biomater. Sci. Polym. Chem. Ed.* **2011**, *22*, 893.
22. Liu, S.; Luo, X.; Zhou, J. In Cellulose—Medical, Pharmaceutical and Electronic Applications; van de Ven T, Godbout L, Eds.; InTech: Croatia, **2013**, p 105. http://dx.doi.org/10.5772/53884.
23. Tang, J.; Myers, M.; Bosnick, K. A.; Brus, L. E. *J. Phys. Chem. B* **2003**, *107*, 7501.
24. Singh, N.; Gareth, J. S.; Jenkins; Bryant, C. N.; Bryce, J. M.; Thierry, G. G. B.; Andy, P. B.; Paul, M. W., Chris, W. J.; Shareen, H. D. *Biomaterials* **2012**, *33*, 163.
25. Chourpa, I.; Douziech-Eyrolles, L.; Ngaboni-Okassa, L.; Fouquenet, J. F.; Cohen-Jonathan, S.; Souce, M.; Marchais, H.; Dubois, P. *Analyst* **2005**, *130*, 1395.
26. Zaitsev, V. S.; Filimonov, D. S.; Presnyakov, I. A.; Gambino, R. J.; Chu, B. *J. Colloids Interface Sci.* **1999**, *212*, 49.
27. Casillas, P. E. G.; Gonzalez, C. A. R.; Pérez, C. A. M. In Infrared Spectroscopy—Materials Science, Engineering and Technology; Theophile, T., Ed.; InTech: Croatia, **2012**. ISBN: 978-953-51–05374. http://www.intechopen.com/books/infrared-spectroscopy-materials-science-engineering-and-technology/infrared-spectroscopy-of-functionalized-magnetic-nanoparticles.
28. Chen, C.; Jiang, X.; Kaneti, Y. V.; Yu, A. *Powder Technol.* **2013**, *236*, 157.
29. Prabhakaran, T.; Hemalatha, J. *Mater. Chem. Phys.* **2013**, *137*, 781.
30. Jiang, L.; Sun, W.; Kim, J. *Mater. Chem. Phys.* **2007**, *101*, 291.
31. Slavov, L.; Abrashev, M. V.; Merodiiska, T.; Ch.Gelev; Vandenberghe, R. E.; Markova-Deneva, I.; Nedkov, I. *J. Magn. Magn. Mater.* **2010**, *14*, 322.
32. Hernandez, R.; Sacristan, J.; Nogales, A.; Fernandez, M.; Ezquerra, T. A.; Mijangosa, C. *Soft Matter.* **2010**, *6*, 3910.
33. Gupta, A. K.; Gupta, M. *Biomaterials* **2005**, *26*, 3995.
34. Sivudu, K. S.; Rhee, K. Y. *Colloids Surf. A: Physicochem. Eng. Aspects* **2009**, *349*, 29.
35. Prozorov, T.; Databy, G.; Gedanken, A. *Thin Solid Film* **1999**, *340*, 191.
36. Kreuter, J. *Pharm. Acta Hel.* **1983**, *58*, 196.
37. Wang, L.; Yang, T.; Yang, J.; Li, Q.; Hao, D.; Yang, J.; Ma, G. *Powder Technol.* **2013**, *235*, 1017.
38. Vilos, C.; Gutiérrez, M.; Escobar, R. A.; Morales, F.; Denardin, J. C.; Velasquez, L.; Altbir, D. *Electron. J. Biotechnol.* **2013**, *16*. DOI: 10.2225/vol16-issue5-fulltext-8. http://www.ejbiotechnology.info.
39. Yang, J.; Park, S. B.; Yoon, H. G.; Huh, Y. M.; Haam, S. *Int. J. Pharm.* **2006**, *324*, 185.
40. Arious, J. L.; Gallardo, V.; Gomez Lopera, S. A.; Plaza, R. C.; Delgado, A. V. *J. Control Release* **2001**, *77*, 309.
41. Starodoubtsev, S. G.; Saenko, E. V.; KHOkhlov, A. R. *Microelectron. Eng.* **2003**, *69*, 324.
42. Debe, M. K. In Handbook of Fuel Cells, Vielstich, W.; Gasteiger, H. A.; Lamm, A., Eds.; John Wiley & Sons: New York, **2003**; Vol. *3*, p 576.
43. Cesar, G.; Gomez; Pastrana, P. G.; Daniel, S.; Estanislao, Z.; Marcelo, A.; Villar; Strumia, C. M. *Polymer* **2012**, *53*, 2949.
44. Oberdoster, G.; Sharp, Z.; Atudorie, V.; Elder, A. C. P.; Gelin, R.; Lunts, A.; Krefing, W.; Cox, C. *J. Toxicol. Environ. Health* **2002**, *65*, 1531.
45. Nita, L.E.; Chiriac, A. P.; Nistor, M. T.; Stoica, I. *Rev. Roum. Chim.* **2011**, *56*, 537.
46. Arruebo, M.; Fernández-Pacheco, R.; Ibarra, M. R.; Santamaría, J. *Nanotoday* **2007**, *2*, 21.
47. Kissel, T.; Roser, M. Proceeding of the International Symposium on Controlled Release of Bioactive Materials, **1991**; Vol. *18*, p 275.
48. Ishihara, K. *Sci. Tech. Adv. Mater.* **2000**, *1*, 131.
49. Hogt, A. H.; Gregonis, D. E. *J. Colloid Interface Sci.* **1985**, *106*, 289.
50. Lj. Tomić, S.; Suljovrujić, E. H.; Filipović, J. M. *Polym. Bull.* **2006**, *57*, 691.